






Phase transitions in a high magnetic field of an odd, symmetric liquid crystal dimer having two nematic phases, N_U and N_{TB} , studied by NMR spectroscopy

C. T. Imrie,¹ D. A. Paterson ,^{1,*} J. M. D. Storey ,¹ C. Chamignon,² M. Lelli ,^{3,†} J. W. Emsley ,^{4,‡} and G. R. Luckhurst ,^{4,§}

¹Department of Chemistry, School of Natural and Computing Sciences, University of Aberdeen, Aberdeen AB24 3FX, United Kingdom

²Centre de RMN à Très Hauts Champs de Lyon (FRE 2034-CNRS, UCB Lyon 1, ENS Lyon), 5 rue de la Doua, 69100 Villeurbanne, France

³Department of Chemistry “Ugo Schiff,” Center for Magnetic Resonance, University of Florence, Sesto Fiorentino (FI) 50019, Italy

⁴School of Chemistry, Faculty of Engineering and Physical Sciences, University of Southampton, Southampton SO17 1BJ, United Kingdom



(Received 19 July 2019; revised 15 June 2020; accepted 31 July 2020; published 28 October 2020)

Both ^1H and ^{13}C NMR spectra have been obtained in a static magnetic field of 23.5 T on a bent-shaped dimer molecule, 1'',7''-bis(4-cyanobiphenyl-4'-yl) nonane (CB9CB), which shows the sequence of liquid crystal phases twist-bend nematic, N_{TB} , and uniaxial nematic, N_U , before entering the isotropic phase. The ^1H spectra are used to locate the temperature at which the sample melts to form a twist-bend nematic, $T_{CrN_{TB}}$, and then $T_{N_{UI}}$ when the isotropic phase is entered, both in a magnetic field of 23.5 T, and to compare these with those measured at the Earth's field. The differences between these transition temperatures are found to be zero within the error in their measurement, in stark contrast to previous measurements by Salili *et al.* [*Phys. Rev. Lett.* **116**, 217801 (2016)]. In the isotropic phase in the presence of the field the sample exists in a paranematic phase in which the molecules of CB9CB are partially ordered. The ^1H and ^{13}C NMR spectra in the paranematic phase are used to measure the critical temperature T^* below which this phase is unstable. The spectra are also used to study the structure, molecular orientational order, and distribution of molecular conformations in the paranematic phase.

DOI: [10.1103/PhysRevE.102.042706](https://doi.org/10.1103/PhysRevE.102.042706)

I. INTRODUCTION

It is well known that the application of just a moderate magnetic field (~ 0.1 T) to a uniaxial nematic phase N_U , having a positive diamagnetic susceptibility anisotropy, $\Delta\chi = \chi_{\parallel} - \chi_{\perp}$, will align the director \mathbf{n} of the phase parallel to the field. There is also another effect, possibly of greater, current interest, namely that the field B will increase the nematic-isotropic temperature $T_{N_{UI}}$ by a small amount depending on a range of macroscopic properties including the field strength. We shall refer to this transition temperature as T_{NI} to simplify the nomenclature and to connect with previous discussions in the literature. Rosenblatt [1] has predicted the shift in the transition temperature δT_{NI} produced by the application of a magnetic field based on a thermodynamic approach. This has the advantage of relating the predicted δT_{NI} to the macroscopic properties of the nematogen. His derivation starts with the differential thermodynamic potential

$$dG_i = -S_i dT - M_i dB, \quad (1)$$

where G_i is the Gibbs potential for phase i either nematic, N_U , or isotropic, I ; S_i is the entropy, and M_i is the magnetization, equal to $\chi_i B$ where χ_i is the susceptibility parallel to the field. This leads to dG in the isotropic and nematic phases which

can be combined at T_{NI} where the differential free energies are the same, thus giving

$$-S_I dT - M_I dB = -S_N dT - M_N dB. \quad (2)$$

Combining the terms in the entropy and those in the magnetization followed by integration of Eq. (2) yields

$$-(S_I - S_N)[T_{NI}(B) - T_{NI}(0)] = (\chi_I - \chi_N)B^2/2. \quad (3)$$

The magnetic susceptibilities χ_I and χ_N for the two phases can be written in terms of the principal components of the susceptibility tensor χ as

$$\chi_I = (\chi_{\parallel} + 2\chi_{\perp})/3 \quad (4)$$

and

$$\chi_N = \chi_{\parallel}. \quad (5)$$

These give

$$\chi_I - \chi_N = -(2/3)\Delta\chi \quad (6)$$

and so the resultant expression for the field-induced shift in the transition temperature is

$$\delta T_{NI} = \Delta\chi B^2/3\Delta S_{NI}. \quad (7)$$

Here

$$\Delta S_{NI} = (S_I - S_N), \quad (8)$$

*Present address: School of Physics and Astronomy, University of Leeds, Leeds, United Kingdom.

†Corresponding author: moreno.elli@unifi.it

‡Corresponding author: jwe@soton.ac.uk

§Corresponding author: G.R.Luckhurst@soton.ac.uk

where I is the initial and N is the final state in accord with convention [2]. The transitional entropy in zero magnetic field, ΔS_{NI} , is readily available. In addition, to predict the shift, δT_{NI} , it is also necessary to know the anisotropy in the magnetic susceptibility, $\Delta\chi = (\chi_{||} - \chi_{\perp})$ for the nematic phase.

By writing the transitional entropy in terms of the enthalpy of transition, ΔH_{NI} , the shift in the transition temperature becomes

$$\delta T_{NI} = T_{NI}(0)\Delta\chi B^2/3\Delta H_{NI}, \quad (9)$$

as found by Rosenblatt [1]. His approach has the benefit of being able to determine the field-induced shift in temperature from quantities which are relatively accessible.

It is interesting to note that the thermodynamic prediction of δT_{NI} is consistent with that based on the Landau–de Gennes theory [3]. This starts with the expansion of the Helmholtz free energy F in terms of the defining order parameter Q of the nematic phase which measures its orientational order; it is related to the principal components of the traceless tensor \mathbf{Q} . The expansion is

$$F = (3/4)a_0(T - T^*)Q^2 - (1/4)bQ^3 + (9/16)cQ^4 - (1/2)\Delta\chi_0 B^2 Q, \quad (10)$$

where a_0 is the leading coefficient, b controls the cubic term and c the quartic; all of these coefficients are taken to be independent of temperature. T^* is the critical temperature below which the isotropic phase is not stable. The magnetic contribution to the free energy is determined by $\Delta\chi_0$, the anisotropy of the magnetic susceptibility for the perfectly ordered uniaxial phase, as well as by Q and B . Minimization of the free energy with respect to the order parameter gives the nematic-isotropic transition temperature in zero field as

$$T_{NI}(0) = T^* + b^2/(27a_0c). \quad (11)$$

The shift in the transition temperature caused by the magnetic field is

$$\delta T_{NI} = 3c\Delta\chi_0 B^2/a_0b; \quad (12)$$

this result can be simplified by using the expression for the transitional enthalpy change ΔH_{NI} , which leads to

$$\delta T_{NI} = T_{NI}(0) Q_{NI} \Delta\chi_0 B^2/3\Delta H_{NI}, \quad (13)$$

where Q_{NI} is the value of Q at T_{NI} . Equation (13) can be restructured to reveal its equivalence to that found by Rosenblatt with his thermodynamic approach [cf. Eq. (9)]. Thus, the product of Q_{NI} and $\Delta\chi_0$ gives the anisotropic magnetic susceptibility of the phase $\Delta\chi$. Additionally, the transitional entropy in zero field, ΔS , is $\Delta H_{NI}/T_{NI}$. Substituting these relations in Eq. (13) gives the thermodynamic result shown in Eq. (9).

In his paper, Rosenblatt [1] estimates the shift in the transition temperature for a magnetic-flux density of 10 T to be of the order of 10^{-3} °C. The specific values of ΔH_{NI} and $\Delta\chi$ employed in this estimation are not given but we take them to be characteristic of a nematogen, such as 4-octyl-4'-cyanobiphenyl (8CB), that Rosenblatt studied experimentally [1]. The Bitter magnet used was capable of reaching fields of about 15 T and in the experiments the field was increased

from 7.3 to 14.8 T. Over this range the transition temperature increased by 1.4×10^{-3} to 5.5×10^{-3} °C; this proved to be in accord with the theoretical predictions.

The small increase in δT_{NI} found by Rosenblatt [1] is in contrast to a much larger value reported in 2008 by Ostapenko *et al.* [3] who studied a bent-core mesogen (BCM), namely 4-chlororesorcinol bis[4-(4-n-dodecyloxybenzoyloxy) benzoate] (CIPbis10bbs). They used a 31-T resistive solenoid which, in their experiments, reached a magnetic field of 30 T, and at this point the shift in the nematic-isotropic temperature was found to be 0.67 °C, clearly significantly larger than that determined for 8CB. A part of this increase can be attributed to the higher magnetic field, but the structure of the BCM, along with its large biaxiality, may also be a significant factor, however, the properties needed to test the predictions of Eq. (9) for CIPbis10bbs do not appear to be available. However, when the properties needed to estimate δT_{NI} are not available the molecular biaxiality can be informative. The expression in Eq. (9) derived by Rosenblatt relates the shift in the transition temperature to the ratio of the anisotropy of the magnetic susceptibility and the transitional enthalpy. According to molecular field theory $\Delta\chi$ is linear in S whereas ΔH_{NI} is quadratic in S so that the ratio $\Delta\chi/\Delta H_{NI}$ is inversely proportional to S . Molecular-field theory also predicts that the orientational order parameter at the N - I transition decreases with the molecular biaxiality [4]. Accordingly, as the molecular biaxiality increases so the shift in the transition temperature might be expected to grow.

A more surprising increase in the field-induced shift in T_{NI} has been reported by Francescangeli *et al.* [5] also using a BCM which was based on 2,5-bis(*p*-hydroxyphenyl)-1,3,4-oxadiazole (ODBP-Ph-OC₁₂H₂₅). This material has a richer phase behavior, but of primary interest are the nematic and smectic- C phases which in zero magnetic field have transition temperatures: T_{NI} of 204 °C and T_{SmCN} of 193 °C. It may also be of relevance that the value of $T_{NI} = 204$ °C is over twice that for CIPbis10bbs (91 °C) [3]. The magnetic field used by Francescangeli *et al.* [5] is fixed at the relatively small value of 1 T. The locations of the two phase transitions were determined from the x-ray scattering patterns of the samples aligned using either the magnetic field or a rubbed polyimide surface in zero field. Despite the relative weakness of the magnetic field it is found that it still increases the two transition temperatures T_{NI} and T_{SmCN} by a remarkable 4 °C. Understanding this result presents a challenge, which is attributed by Francescangeli *et al.* to the presence of so-called cybotactic clusters of the curved molecules of ODBP-Ph-OC₁₂H₂₅ [5].

A more recent study of the effect on transition temperatures of applying a magnetic field has been reported by Salili *et al.* [6], based on three liquid crystal dimers which form both nematic N_U and twist-bend nematic N_{TB} phases. One of the dimers of primary interest to the present study is 1'',7'''-bis(4-cyanobiphenyl-4'-yl) nonane (CB9CB). The spacer linking the two-mesogenic groups of the dimer contains an odd number of methylene groups and so on average the dimer has a curved shape, as shown in Fig. 1, which is also the case for the BCM systems studied by Ostapenko *et al.* [3] and Francescangeli *et al.* [5].

In the work by Salili *et al.* [6] the maximum field of the split-helix resistive solenoid magnet is 25 T and the transition

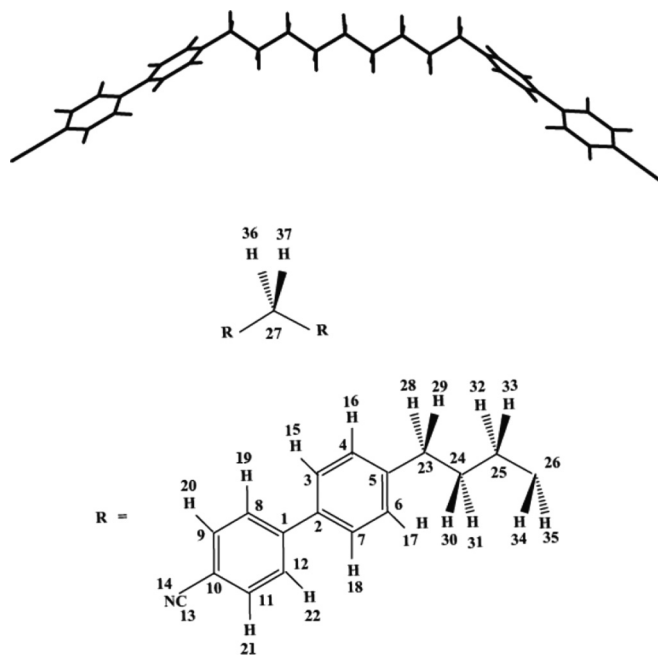


FIG. 1. Structure (top) and atomic labeling of the symmetric liquid crystal dimer CB9CB.

temperatures T_{NI} were monitored by observing changes in the effective birefringence. Remarkably the shift in T_{NI} for CB9CB was found to be about 13 °C, and also surprising is that the shift in the transition temperature was found to be linear in the magnetic field unlike the theoretical predictions [1,3,7] and previous experimental measurements [1,5] where they are quadratic. Salili *et al.* [6] hypothesized that this unexpected behavior could be a consequence of a change of the average molecular structure from bent to linear.

In addition to the use of experiments to explore the influence of magnetic fields on the nematic-isotropic transition temperatures there are, as we have seen, also theoretical approaches such as molecular-field [7] and Landau-de Gennes [3,5,7] theories. As well as these approaches it is possible to employ Monte Carlo computer simulation methodology to obtain a potentially more reliable understanding of the way in which the shift, $\delta T_{NI}(T)$, depends on the molecular structure as well as specific interactions. One such study has been undertaken by Ghoshal *et al.* [8] using a simple cubic lattice model analogous to that developed by Lebwohl and Lasher [9]. Here the interactions between the uniaxial, oblate molecules are confined to nearest neighbors and take a particularly simple, second-rank form [8,9]. Added to this potential is a term representing the interaction between a molecule and an external magnetic field. This was given the form

$$U_j^{\text{field}} = -\varepsilon\xi[(3/2)(\mathbf{w}_j \cdot \mathbf{z})^2 - (1/2)], \quad (14)$$

where ε is related to the strength of the anisotropic molecular interactions, and \mathbf{w}_j is the orientation of a vector in molecule j which interacts with the magnetic field aligned along the lattice Z axis and denoted by \mathbf{z} . The strength of the magnetic field interaction is given by

$$\xi = \Delta\chi_{\text{mol}}B^2/3\mu_0\varepsilon, \quad (15)$$

where $\Delta\chi_{\text{mol}} = (\chi_{\parallel} - \chi_{\perp})_{\text{mol}}$ is the anisotropy in the molecular magnetic susceptibility, and μ_0 is the permeability of free space [cf. Eqs. (3) and (10)]. As well as using a system of uniaxial molecules, a set of biaxial molecules having D_{2h} point-group symmetry was also studied. Their biaxiality is denoted by λ which is related to the principal components of the molecular polarizability tensor α . Here λ is $\sqrt{(3/2)(\alpha_2 - \alpha_1)/(2\alpha_3 - \alpha_1 - \alpha_2)}$ and, for D_{2h} oblate molecules, passes from 0 to a maximum of $1/\sqrt{6}$ in the molecular biaxiality. In the simulations by Ghoshal *et al.* [8] λ was equal to the modest value of 0.2.

The largest systems used in the MC simulations contained 40^3 particles and they were performed over a narrow temperature range in the vicinity of T_{NI} within which the system remains uniaxial. The shift in the transition temperature, δT_{NI} , caused by the applied magnetic field increases until the growth stops at a critical value ξ_C when the nematic and paranematic phases are equivalent. This behavior is predicted by molecular-field theory [7] as is the reduction in ξ_C with the molecular biaxiality; indeed, this shows that for the maximum biaxiality the nematic-paranematic transition reaches a critical point. What is not predicted by molecular-field theory is that the dependence of δT_{NI} on the magnetic field found by the simulations is greater than quadratic. In addition, the increase in δT_{NI} with the field is greater for the biaxial than the uniaxial molecules.

Intrigued by this diverse set of experimental, theoretical, and simulation results for the influence of a magnetic field on the nematic-isotropic transition temperature it was decided to record ^1H and ^{13}C NMR spectra of CB9CB (see Fig. 1) at a constant magnetic field of 23.5 T; this is one of the compounds studied by Salili *et al.* [6]. The transition temperatures for our sample of CB9CB in the Earth's magnetic field are Cr 86 °C N_{TB} 108 °C N_U 124 °C I [10], which are comparable to those reported by Salili *et al.* [6].

The main advantages in using NMR spectroscopy to study the effect on a liquid crystal of an applied magnetic field are first that the sample is in a uniform magnetic field and is free from any competing effects of surface forces on the director alignment, and second both ^1H and ^{13}C spectra can be recorded at temperatures above T^* in the paranematic phase. In this pretransitional region the presence of a magnetic field induces residual dipolar couplings $D_{i,j}^B$ for several sites in the molecules [11,12], and their temperature dependence in the pretransitional region allows a value of T^* to be obtained for this curve-shaped nematogen. The values of the $D_{i,j}^B$ also allow order parameters $S_{\alpha\beta}^B$ induced by the magnetic field \mathbf{B} within the sample to be obtained for rigid fragments such as the phenyl groups and for each CH_2 group in the flexible nonane spacer. The values of $S_{\alpha\beta}^B$ can also be used to test models for the conformations adopted by the flexible nonane spacer when the orientational order of the molecules is close to zero. Note that although CB9CB does form the twist-bend nematic phase a direct study of this does not form part of our investigation. It should also be noted that in two molecules with similar bent-shaped structures, there is evidence for a splay-bend nematic phase between a twist-bend and a normal uniaxial nematic phase [13,14]. However, in both molecules the transition to the isotropic phase is from a N_U phase.

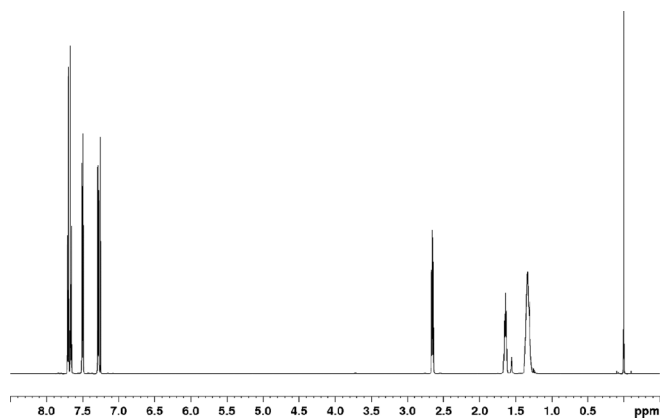


FIG. 2. 600-MHz ^1H spectrum of CB9CB, acquired at 14.1 T. The spectrum scale is reported in ppm with respect to the TMS reference at 0.00 ppm.

The layout of our paper is as follows. Section II describes how the NMR spectra were obtained and assigned within the temperature range $\sim 50^\circ\text{C}$ to 145°C . The accuracy with which the temperature of the sample can be set in this range is a vitally important aspect of these experiments, and the calibration procedure is described here in detail. Section III describes how the change from very broad ^1H to very narrow resonance absorptions is used to detect the transition to the isotropic phase at T_{NI} . In Sec. IV the ^1H and ^{13}C spectra obtained on cooling in the paranematic phase are described, and in Sec. V the induced residual dipolar couplings (RDCs) obtained are used to locate T^* . Section VI shows how the RDCs obtained at a fixed temperature in the paranematic phase are used to obtain molecular orientational order parameters, the structure of the biphenyl group, and how the distribution of conformers of the nonane spacer chain is characterized. Our conclusions are summarized in Sec. VII.

II. NMR EXPERIMENTS

A. Assignment of ^1H and ^{13}C resonances of samples in isotropic phases

The main aim is to assign resonances in the spectra obtained at 23.5 T of a sample of pure CB9CB in the isotropic phase. This task was achieved by first recording ^1H and ^{13}C spectra on a sample of CB9CB dissolved in CDCl_3 on a 600-MHz Bruker spectrometer equipped with a TCI 5-mm cryoprobe. The 600-MHz proton spectrum was recorded with a single repeated pulse sequence with a 90° pulse angle, 128 scans were collected in 1.96-s acquisition time (recovery delay, 1.04 s). The spectra are shown in Figs. 2 and 3. The chemical shifts and scalar coupling constants obtained from these spectra are given in Tables I and II.

A one-dimensional (1D) ^{13}C NMR spectrum was recorded with a power-gated proton decoupling sequence and a 90° ^{13}C pulse angle, and 1024 free induction decays (fids) were collected. Each fid was acquired in 1.10 s with a recovery delay 8.90 s before a scan. The spectrum is shown in Fig. 4. The chemical shifts of the ^{13}C nuclei are given in Table III.

The linewidths in these spectra of the sample dissolved in CDCl_3 are an order of magnitude smaller than those of

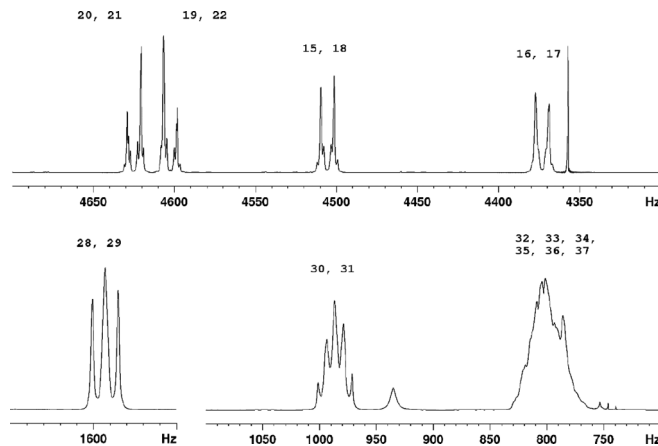


FIG. 3. Enlargements of the 1D ^1H spectrum of CB9CB shown in Fig. 2. On the top of each peak the ^1H assignment with the atomic positions of Fig. 1 is reported. To highlight the J coupling between peaks, the x axis is reported in Hz with respect to the TMS reference at 0.00 Hz. The spectrum is processed with a Gaussian window function ($\text{GB} = 1.0$ and $\text{LB} = -0.5$ Hz) to better detail the J -coupling fine structure.

the spectra of pure CB9CB leading to much better signal-to-noise ratios and making possible the recording of various 2D correlation spectra. A ^1H gCOSY 2D NMR experiment [15] was performed with 4096 real points in the direct dimension (F_2), acquiring four scans for each of 1024 indirect (F_1) t_1 increments, with spectral widths of 5102 Hz in both F_2 and F_1 . The overall F_1 acquisition time was 401 ms and a recycle delay of 3.0 s was used. A ^1H - ^{13}C gHSQC 2D NMR experiment [16] was acquired with 2048 real points with four scans for each of 2048 t_1 increments, with spectral widths of 8403 Hz in F_2 and 41067 Hz in F_1 . The overall indirect acquisition time was 122 ms with a recycle delay of 1.38 s. A ^1H - ^{13}C gHMBC 2D NMR experiment [17] was acquired with 3072 real points with 16 scans for each of 1024 t_1 increments with spectral widths of 9014 Hz in F_2 and 31746 Hz in F_1 . The overall acquisition time was 170 ms with a recycle delay of 1.33 s.

The assignment information gained from the experiments on the spectra of the sample of CB9CB dissolved in CDCl_3 at 600 MHz and 298 K formed a basis for analyzing a 2D gradient-INADEQUATE spectrum [18] obtained for pure CB9CB in the isotropic phase at 135°C . The spectrum shown

TABLE I. Values of the ^1H chemical shifts for a sample CB9CB dissolved in CDCl_3 in ppm at 298 K relative to the internal TMS reference.

Nucleus	Chemical shift/ppm
32–37	1.25–1.40
30,31	1.64
28,29	2.65
16,17	7.28
15,18	7.50
19,22	7.66
20,21	7.70

TABLE II. Values of the ^1H - ^1H J -coupling constants (Hz) obtained from the sample of CB9CB dissolved in CDCl_3 at 600 MHz and 298 K.

ij	$J_{ij}/(\text{Hz})$
30,32	7.4 ± 0.2
30,28	7.8 ± 0.1
16,15	8.3 ± 0.1
19,20	8.4 ± 0.1

in Fig. 5 was acquired at 23.5 T (1000 MHz) on the pure liquid crystal sample in the isotropic phase at 135 °C. The ^{13}C 90° pulse was $15.75 \mu\text{s}$, and a ^1H WALTZ decoupling sequence of 4.166 kHz was used for the duration of the pulse sequences and the acquisition times. A total of 4096×126 real points was acquired in the direct and indirect dimensions, respectively. The acquisition times were 32.768 and 0.6930 ms for the direct and indirect dimensions, respectively, with 192 scans per increment and 50 s of recycle delay. The spectrum was processed in magnitude mode. The assignment of the ^{13}C resonances using the 2D INADEQUATE spectrum followed the pathway indicated in Figs. 6(a)–6(c).

In an INADEQUATE spectrum each pair of directly connected ^{13}C carbons, C_i and C_j , which share a one-bond scalar coupling, $^1J_{ij}$, give a pair of doublets centered at the chemical shifts δ_i and δ_j in the dimension F_2 . This pair of doublets generate a pair of crosspeaks with the same frequency in the indirect dimension, F_1 , which corresponds to the sum of the chemical shifts, δ_i and δ_j , of the two ^{13}C spins. Starting from the cross peak associated to the carbon-1 nucleus (280 and 144 ppm) (^{13}C assigned following the numbers in Fig. 1) in Fig. 6(c), moving horizontally we find the cross peak of the coupled carbon-2 (280 and 135 ppm). Conversely, moving vertically we find another cross peak (270 and 144 ppm) with the same chemical shift of carbon-1 but is horizontally coupled to carbon-8 and carbon-12.

Thus, each pair of directly connected carbons generated a pair of cross peaks horizontally aligned while along the vertical direction we can connect one coupled pair to another

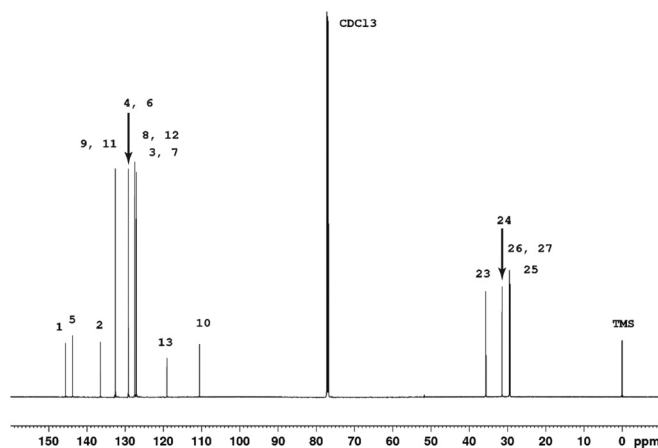


FIG. 4. 150-MHz ^{13}C - $\{^1\text{H}\}$ spectrum of CB9CB dissolved in CDCl_3 , acquired at 14.1 T. The spectral scale is reported in ppm with respect to the TMS reference at 0.00 ppm. On the top of each peak is the ^1H assignment with the atomic positions of Fig. 1 reported.

TABLE III. The ^{13}C chemical shifts (ppm relative to TMS) obtained from the 150-MHz spectrum of CB9CB dissolved in CDCl_3 at 298 K.

Nucleus	Chemical shift/ppm
25	29.30
26	29.48
27	29.49
24	31.39
23	35.63
10	110.56
13	119.03
3,7	127.08
12,8	127.47
4,6	129.18
9,11	132.56
2	136.47
5	143.76
1	145.60

pair sharing the same nucleus. On this basis, moving zigzag horizontally and vertically following the red dashed line in Fig. 6(c) we can assign the whole carbon backbone of the molecule. For example, from position 1 in Fig. 6(c) we can assign horizontally the chemical shift of carbon-2, then moving vertically following the red dashed line we find a cross peak (260 and 135 ppm) which is horizontally coupled with carbons-3,7 (260 and 126 ppm). We can then move vertically and we find the couple of cross peaks corresponding to the pair of carbons 3,4 and 6,7, and again horizontally we determine the shift of carbon, 4,6. The path can be followed until the whole carbon backbone is assigned. The assignment thus obtained was confirmed with that determined using experiments on the sample dissolved in CDCl_3 solution at 25 °C. This comparison also made it possible to precisely assign carbon 26 and 27 that are poorly resolved in the INADEQUATE spectrum. The chemical shifts reported in Table III refer to the solution of CB9CB in CDCl_3 at 25 °C and may differ slightly from those obtained from the INADEQUATE spectrum on pure CB9CB at 135 °C.

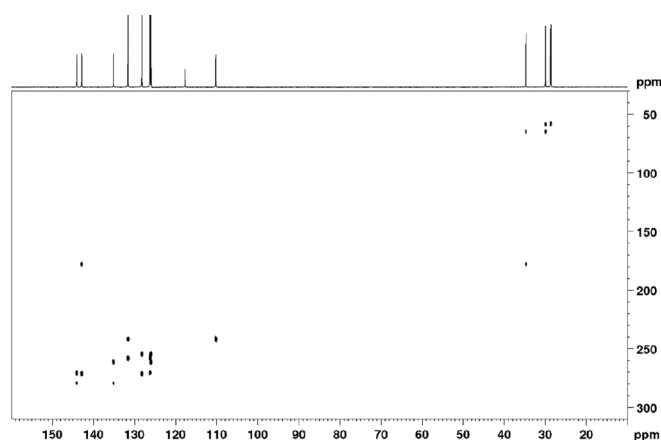


FIG. 5. 250-MHz ^{13}C - ^{13}C INADEQUATE spectrum of pure CB9CB at 23.5 T in the isotropic phase at 135 °C.

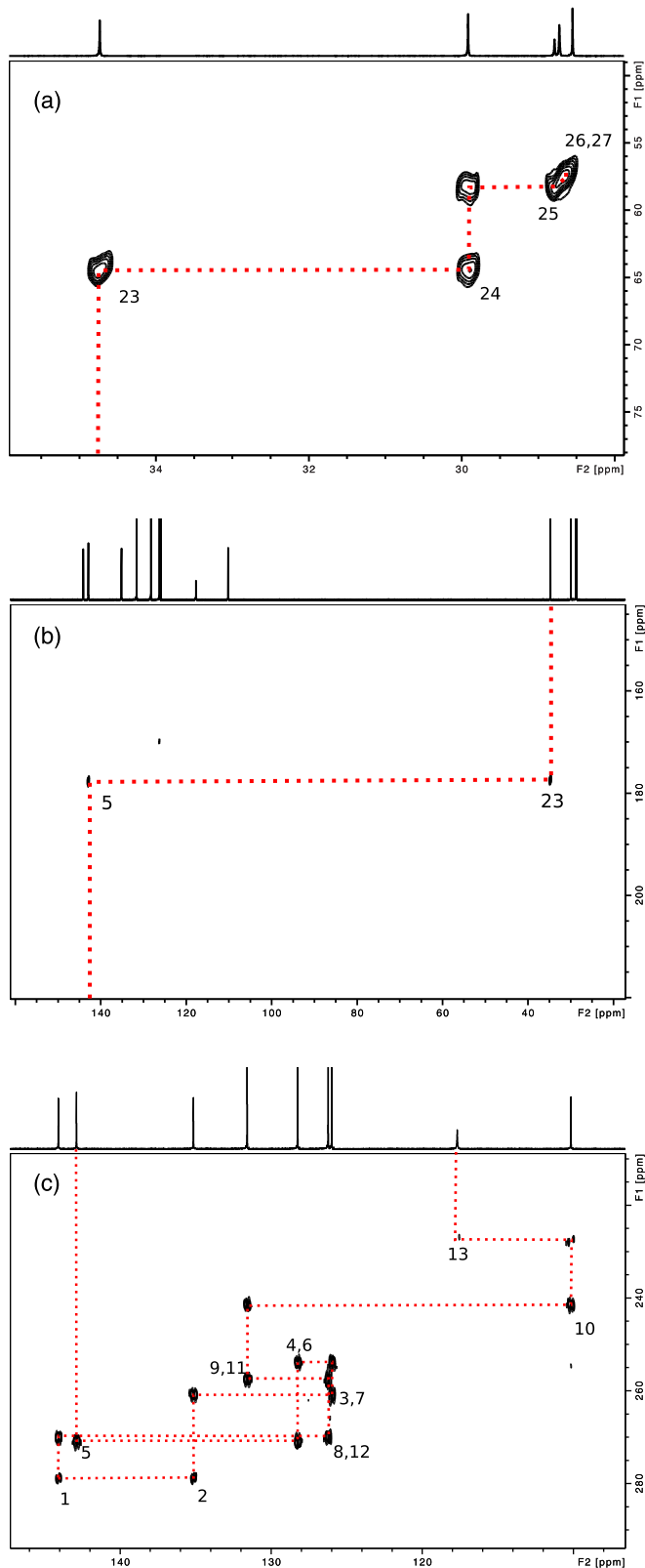


FIG. 6. Assignment pathway of the ^{13}C - ^{13}C INADEQUATE spectrum shown in Fig. 5. Three different enlargements (a)–(c) are reported. A red dotted line highlights the assignment pathway from one cross peak to another. Numbers report the assigned cross peaks with the positions given in Fig. 1.

B. NMR spectra obtained on a pure sample of CB9CB

The ^1H and ^{13}C spectra of CB9CB in its liquid crystal and isotropic phases were recorded on a Bruker Avance III spectrometer at a fixed magnetic field of 23.5 T at the High Field NMR Centre in Lyon using a standard 5-mm double resonance broadband (BBO) probe. The sample was contained in the outer annulus of a Wilmad coaxial tube of type WGS-5BL, which has a 5 mm o.d. and an inner coaxial tube of 2 mm o.d. The inner tube contained $\text{DMSO-}d_6$, which was used to provide a deuterium signal for field-frequency locking. Temperature variation and control of the sample was by heating a stream of N_2 gas which passed over the sample. The temperature is controlled to ± 0.1 °C using a PT100 resistor located inside the probe, close to the sample. As the resistor is external, there is a difference between the temperature measured and that inside the sample tube; for this reason the temperature calibration described here is performed in order to compensate for this temperature difference and to provide an accurate measurement of the effective sample temperature. The calibration of the temperature sensor of the instrument was made on the basis of the chemical shift difference, $\Delta\delta$, for the two proton signals observed with the standard sample of 80% ethylene glycol in $\text{DMSO-}d_6$ ($\Delta\delta$). This difference is related to the sample temperature by [19]

$$T_{\text{sample}}(\text{K}) = -108.33 \times \Delta\delta(\text{ppm}) + 460.41. \quad (16)$$

The temperature inside a NMR sample tube depends on the rate of flow of the heating nitrogen gas, and the position of the tube in the spectrometer probe, and these factors must be the same when measuring $\Delta\delta$ on the standard sample and the NMR spectra of CB9CB. To produce a high stability of the temperature inside the standard sample, it was left for more than one hour in the probe at each of the three temperatures 144 °C, 121 °C, and 72 °C before measuring the chemical shift difference between ethylene glycol protons for calibration. With the values obtained, a temperature calibration curve was produced by a procedure described in the Bruker Variable Temperature User Manual [19]. This temperature calibration was confirmed by using another sample, composed of pure ethylene glycol without solvent, following the calibration curve reported in the literature [20]. The temperatures calibrated using these two standards differ by <0.1 °C confirming the accuracy of the method described above. In practice the setting accuracy of the temperature when recording the spectra of the sample of CB9CB in liquid crystal phases is estimated to be of the order of 0.5 °C [20], with a long-term stability of better than 0.1 °C (Bruker spectrometer specifications).

Proton spectra were first recorded automatically on heating the sample from ~ 70 °C to 145 °C in steps of 2 °C, waiting 30 min for thermal equilibrium to be reached. The ^1H NMR spectra when the sample is in the solid or the two nematic phases are spread over ~ 40 kHz. The solution NMR probe used here to have optimal temperature control cannot withstand the required rf power at 1000 MHz to excite uniformly the protons over this broad frequency range with a 90° excitation pulse. To record the ^1H NMR spectra with uniform excitation was achieved by application of single, repeated 30° pulses each of 5.5 μs duration. Each spectrum is the result of averaging

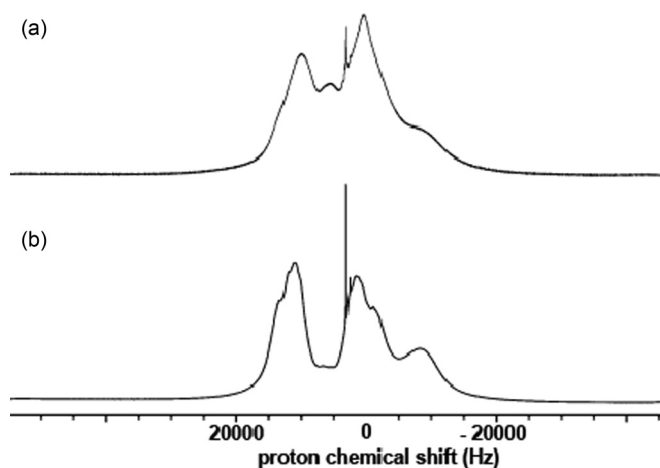


FIG. 7. 1000-MHz ^1H spectrum of CB9CB observed close to the melting point. The narrow peaks near the center of the spectra are from a proton impurity in the $\text{DMSO-}d_6$ sample which is contained in the inner, coaxial tube. Spectrum (a) was recorded at 83 °C when the sample is in the solid phase, and (b) at 85 °C when the sample is in the twist-bend nematic phase.

64 fids each with a 0.164-s acquisition time (relaxation delay, 1.5 s). A 1-Hz line broadening was applied before Fourier transformation. ^1H chemical shifts are referenced to the deuterium $\text{DMSO-}d_6$ signal (2.49 ppm).

III. DETECTION OF THE PHASE TRANSITIONS

The phase transition from the solid to a liquid crystal produces a change in the broad line shape at between 83 ° and

85 °C compared with the melting point of 86 °C characterized by differential scanning calorimetry with a value for the enthalpy of melting of 0.72 kJ mol^{-1} [10] and a transitional entropy, $\Delta S/R$, of 0.33. Spectra below and above the melting transition are shown in Fig. 7.

Above 85 °C until the transition to the isotropic phase at ~ 123 °C the broad resonance absorption retains the same shape, but varies in width as the temperature is increased. There is a small, gradual increase in width until ~ 109 °C followed by a decrease until the isotropic phase is reached.

Salili *et al.* [6] found that their sample of CB9CB became isotropic in a field of 22 T at ~ 140 °C, and guided by this result our sample continued to be heated, while recording proton spectra at 2 °C intervals until ~ 5 °C above this temperature. The transition to the isotropic phase for our sample of CB9CB was marked by a dramatic decrease in the overall width of the ^1H spectra and the appearance of sharp lines above ~ 123 °C.

IV. ^1H AND ^{13}C NMR SPECTRA ABOVE T_{NI} IN THE PARANEMATIC PHASE

Proton and carbon spectra were recorded automatically on cooling the sample from 130 °C to 123 °C in steps of 0.3 °C, and then down to 121.8 °C in steps of 0.2 °C, waiting 10 min after each temperature step for thermal equilibrium to be reached. Below 121.8 °C the sample is completely in the N_{U} phase. ^1H NMR spectra were recorded with a single, repeated pulse sequence with a ^1H 30° excitation angle pulse of 5.5 μs (^1H 90° pulse 16.5 μs), eight scans per spectrum, and an acquisition time of 1.818 s (recycling delay, 1.5 s), and ^{13}C NMR spectra were acquired with a single repeated pulse experiment with a short excitation pulse of 3.0 μs (^{13}C 90°

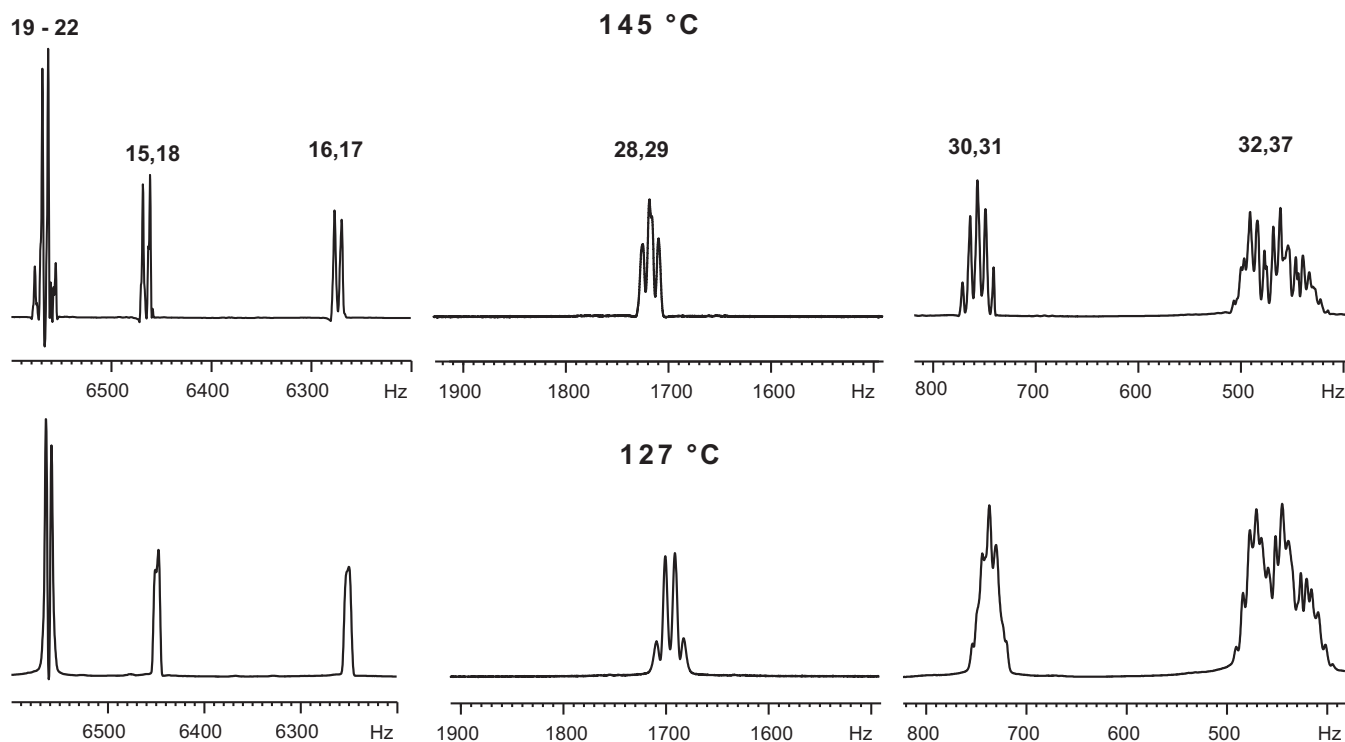


FIG. 8. 1000-MHz ^1H spectra of CB9CB observed in the paranematic phase at 145 °C and 127 °C.

pulse 15.75 μ s), and the acquisition time was 1.049 s. A total of 1024 fids were collected each with a recycle delay of 0.2 s, and averaged before Fourier transformation to give the spectra. The ^1H spectrum obtained at 145 $^\circ\text{C}$ is shown in Fig. 8 together with a spectrum recorded after cooling to 127 $^\circ\text{C}$.

The ^1H spectra of the sample change slowly on lowering the temperature from 145 $^\circ\text{C}$ as residual dipolar couplings D_{HH}^B induced by the magnetic field grow in magnitude in the paranematic phase. These residual dipolar couplings add to the scalar couplings $J_{i,j}$ to give total spin-spin couplings $T_{i,j}$:

$$T_{i,j} = J_{i,j} + 2D_{i,j}^B. \quad (17)$$

By 127 $^\circ\text{C}$ the values of $D_{i,j}^B$ are noticeably affecting the ^1H spectrum, as seen in Fig. 8. Thus the doublet splittings on peaks 15,18 and 16,17 have a separation of ~ 7.0 Hz at 145 $^\circ\text{C}$, but these have become broad singlets at 127 $^\circ\text{C}$ as the values of $D_{15,16}^B = D_{17,18}^B$ change from ~ 0 to ~ -7 Hz. The negative signs of $D_{15,16}^B = D_{17,18}^B$ reveal that S_{zz}^B , the field-induced order parameter for an axis fixed parallel to the C1–C2 direction of the cyanobiphenyl groups, is positive. The sign of S_{zz}^B is determined by that of $\Delta\chi_{zz}$, the component along the z axis of the anisotropy of the molecular magnetic susceptibility.

Below ~ 127 $^\circ\text{C}$ the peaks in the ^1H spectra broaden further. In the small interval from 123 to 122.6 $^\circ\text{C}$ there is a rapid increase in the doublet splitting from peaks for protons 28 and 29, as shown in Fig. 9; then at 122.4 $^\circ\text{C}$ a small amount of the signal from the liquid crystal phase appears, which grows at temperatures down to 121.8 $^\circ\text{C}$ when only a trace remains of the isotropic phase. The splitting of the doublet is $\sim 3D_{28,29}^B$.

Examples of ^{13}C spectra recorded on cooling in the paranematic phase are shown in Fig. 10. The ^{13}C spectra are essentially unchanged until ~ 123 $^\circ\text{C}$ when the values of $D_{\text{C}_i\text{H}_j}^B$ begin to increase together with broadening of the peaks. On cooling slowly the sample froze at ~ 57 $^\circ\text{C}$ compared to the melting point of ~ 84 $^\circ\text{C}$ found on heating from the solid phase.

V. MEASUREMENT OF THE CRITICAL TEMPERATURE T^*

The values of both $D_{\text{H}_i\text{H}_j}^B$ and $D_{\text{C}_i\text{H}_j}^B$ are predicted to depend upon temperature in the same way [21], namely

$$D_{\text{H}_i\text{H}_j}^B = A_{\text{HH}}/(T - T^*), \quad (18)$$

$$D_{\text{C}_i\text{H}_j}^B = A_{\text{CH}}/(T - T^*); \quad (19)$$

here T^* is the critical temperature introduced in Eq. (10).

The dipolar couplings in the paranematic phase given by the relationships in Eqs. (18) and (19) are predicted to hold strictly only for nematogens which are rigid and axially symmetric. The molecule CB9CB is certainly nonrigid, and probably exists as a distribution of conformers each of which is strongly biaxial. In practice the dependence on temperature close to T_{NI} of values for both $D_{\text{H}_i\text{H}_j}^B$ and $D_{\text{C}_i\text{H}_j}^B$ are in good agreement with Eqs. (18) and (19). The temperature dependencies of all nine values of $D_{\text{C}_i\text{H}_j}^B$ are shown in Fig. 11, and the results of fitting each coupling to Eq. (19) by a nonlinear, least-squares procedure are given in Table IV. The nine values

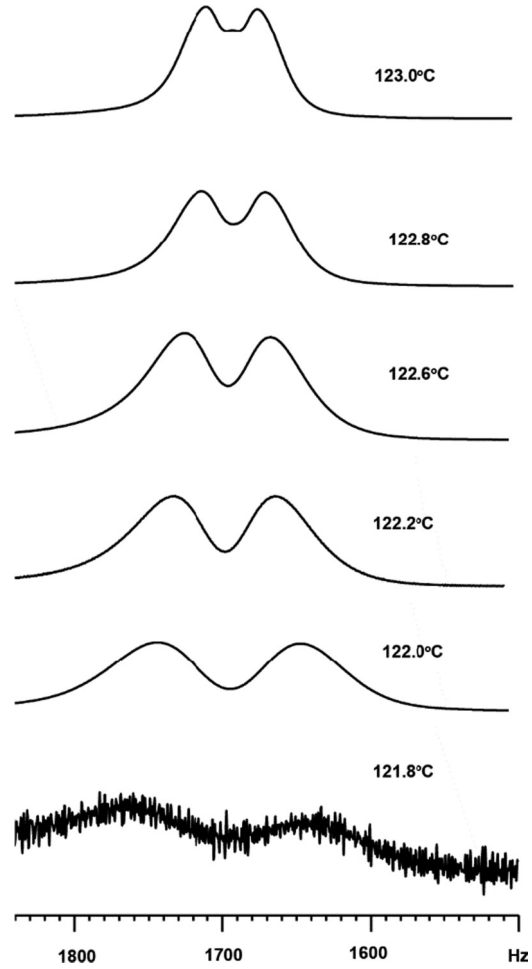


FIG. 9. The growth in the doublet splitting on the peak from H28 and H29 as the transition to the nematic phase of CB9CB is approached in the paranematic phase. At 121.8 $^\circ\text{C}$ the sample shows spectra from both the paranematic and nematic phases with most of the sample being in the nematic. The spectrum for the nematic phase is not shown.

of T^* were then averaged to give a value for T^* of 394.49 ± 0.05 K.

Only one proton-proton field-induced coupling, $D_{28,29}^B$, could be extracted from the ^1H spectra close to T_{NI} for use in obtaining a value for T^* , as shown in Fig. 12.

The data for $D_{28,29}^B$ gave $T^* = 394.36 \pm 0.05$ K, which is equal to within experimental error to the average of the nine sets of values of $D_{\text{C}_i\text{H}_j}^B$, as expected [21]. Taking $T_{\text{NI}} = 395.4$ K to be when the presence of the liquid crystal signal is first detected in the ^1H spectrum on cooling gives the mean value of the difference, $T_{\text{NI}} - T^*$, to be 0.9 ± 0.1 $^\circ\text{C}$. Wiant *et al.* [22] have reported that $T_{\text{NI}} - T^*$ for 16 different monomeric calamitic liquid crystals has a mean value of 1.7 $^\circ\text{C}$, while for a bent-core compound they measured a value of 0.38 ± 0.02 $^\circ\text{C}$. Attard *et al.* [23] measured $T_{\text{NI}} - T^*$ for the nematogen 5CB by deuterium NMR to be 0.9 $^\circ\text{C}$. Values of the difference $T_{\text{NI}} - T^*$ for other bent as well as Z-shaped liquid crystal dimers have been measured previously and are given in Table V, and their structures are compared with CB9CB in Fig. 13.

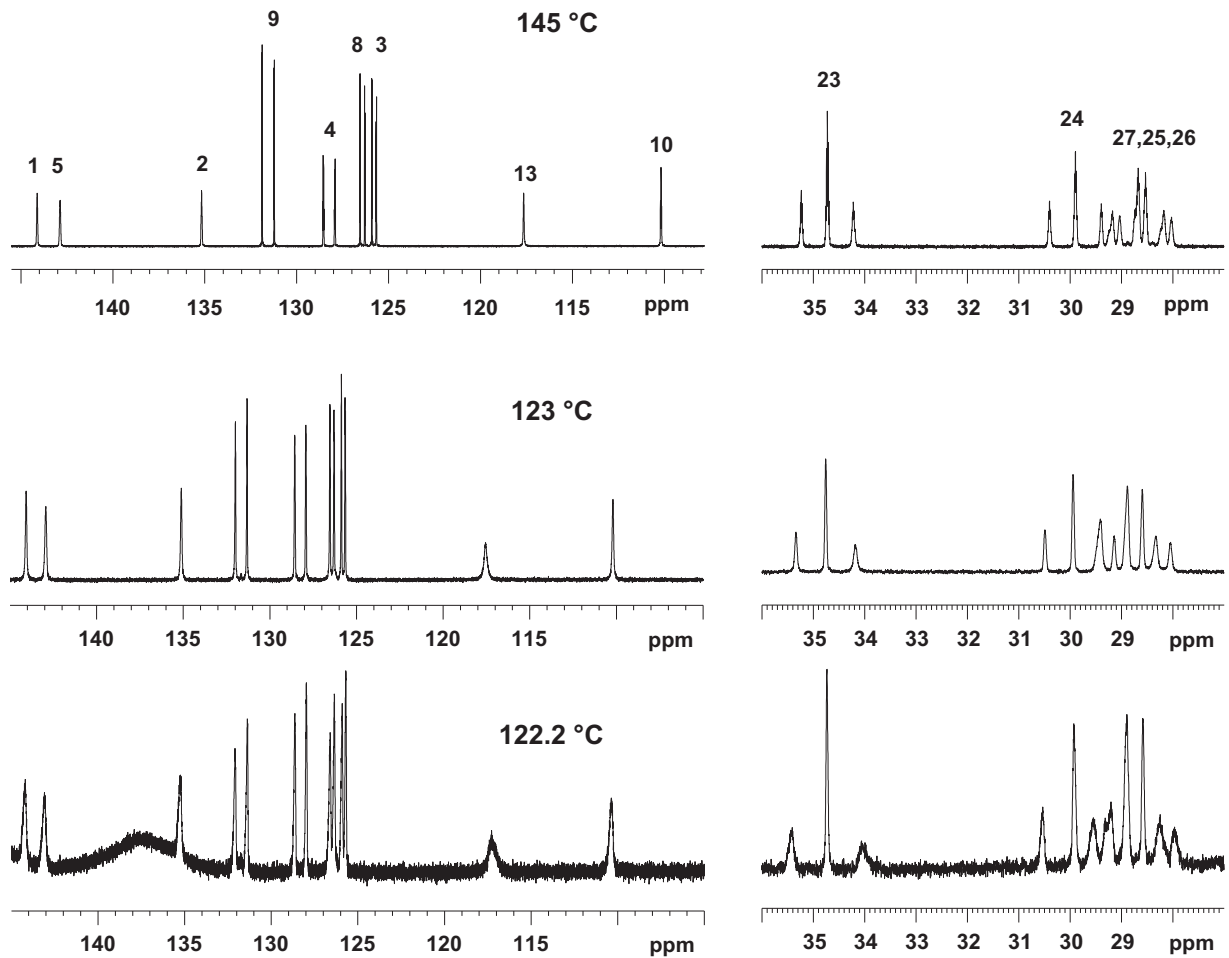


FIG. 10. 250-MHz ^{13}C NMR spectra of CB9CB recorded in the paranematic phase in a field of 23.5 T.

The results for the transitional entropy and the temperature difference shown in Table V for a range of nematogens suggest that $\Delta S_{\text{NI}}/R$ increases with $(T_{\text{NI}} - T^*)$. This empirical

dependence is apparent in Fig. 14, although more results are needed to test this in detail. However, a more formal relationship may be obtained from the Landau-de Gennes theory starting from Eq. (11) where the magnetic term has been removed. This can be rearranged to give the temperature

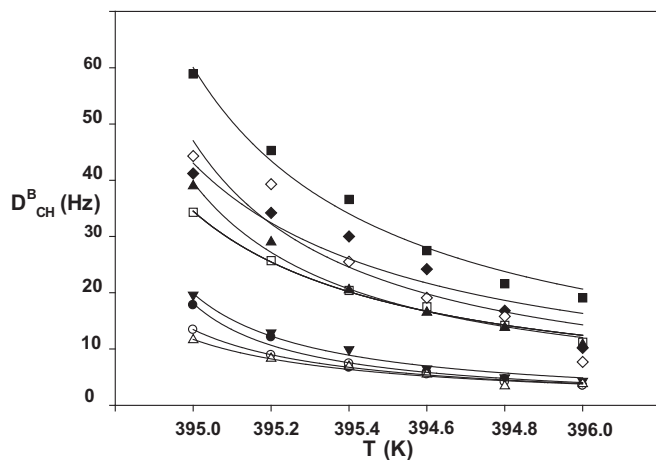


FIG. 11. The dependence of each value of D_{CH}^B on temperature for CB9CB observed in the paranematic phase with a magnetic field of 23.5 T. The solid lines show the best, least-squares fits of the experimental values to Eq. (19). The points are ■ C23; ◇ C25; ◆ C27; ▲ C26; □ C24; ▼ C8; • C9; ○ C4; △ C3.

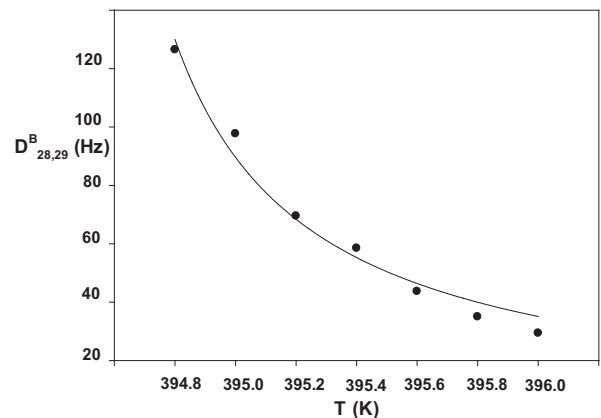
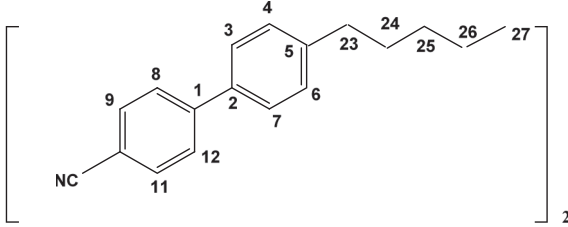


FIG. 12. Temperature dependence of $D_{28,29}^B$ (•) close to T_{NI} for CB9CB at a field of 23.5 T. The solid line shows the best fit to Eq. (18).

TABLE IV. The parameters A_{C_iH} /Hz and T^*/K obtained for the different sites in CB9CB by a nonlinear, least-squares fitting procedure.



Site i	9	8	3	4	23	24	25	26	27
A_{C_iH}	5.2 ± 0.6	6.6 ± 0.6	5.6 ± 0.6	5.4 ± 0.4	31.5 ± 2.5	19.4 ± 0.9	20.5 ± 4.8	17.3 ± 1.1	26.3 ± 5.7
T^*	$394.60 \pm .04$	394.68 ± 0.04	394.52 ± 0.06	394.60 ± 0.03	394.48 ± 0.05	394.44 ± 0.03	394.6 ± 0.1	394.56 ± 0.03	394.4 ± 0.2

difference as

$$(T_{NI} - T^*) = b^2/27a_0c. \tag{20}$$

The transitional entropy may also be obtained in our notation from the enthalpy of transition as [28]

$$\Delta S_{NI} = a_0b^2/27c^2. \tag{21}$$

Eliminating b^2 from both equations gives the relationship between them as

$$(T_{NI} - T^*) = c\Delta S_{NI}/a_0^2; \tag{22}$$

this is broadly in keeping with the results in Fig. 14. For this to be true the ratio c/a_0^2 should be the same for the different nematogens. It is perhaps more interesting to remove the term in c from Eqs. (20) and (21) which leads to

$$(T_{NI} - T^*)^2 = b^2\Delta S_{NI}/27a_0^3. \tag{23}$$

The Landau–de Gennes theory is now seen to predict that the transitional entropy is quadratic in the temperature difference, a result which does not appear to be consistent with the experimental results in Fig. 14; in addition the ratio b^2/a_0^3 should exhibit a universality. A more detailed set of results is needed to test both the Landau–de Gennes predictions. It would be interesting to explore whether the tendency of $T_{NI} - T^*$ to vary linearly with the change in entropy at T_{NI} is observed for other mesogens.

VI. DEPENDENCE OF THE FIELD-INDUCED DIPOLAR COUPLINGS ON STRUCTURE, ORIENTATIONAL ORDER, AND CONFORMATION

The molecules in liquid crystal phases are moving rapidly, but not randomly, as whole entities, and there is also internal motion between N_{conf} conformations, which is usually also sufficiently rapid that the observed dipolar couplings $D_{i,j}$ between nuclei in uniaxial liquid crystal phases are averages over both types of motion to give

$$D_{i,j} = \sum_n P_{LC}(n)D_{i,j}(n). \tag{24}$$

Here $P_{LC}(n)$ is the probability that a molecule is in the n th conformation with a dipolar coupling $D_{i,j}(n)$, which is related

TABLE V. Values of $(T_{NI} - T^*)/^\circ C$ and $\Delta S_{NI}/R$ for some bent-shaped and Z-shaped mesogens.

Mesogen	$T_{NI}/^\circ C$	$(T_{NI} - T^*)/^\circ C$	$\Delta S_{NI}/R$	Ref.
CB9CB	124	0.9 ± 0.1	0.33	This work
BCBO9	173	4.8 ± 1.0	0.94	[24]
BCBO10	186	14.8 ± 0.5	2.14	[24]
CIPbis10BB	76.5	0.38 ± 0.02	0.37	[22,25]
5-9-5	131.3	1.1 ± 0.3	Not available	[26]
5-10-5	149	8.5	2.16	[26,27]

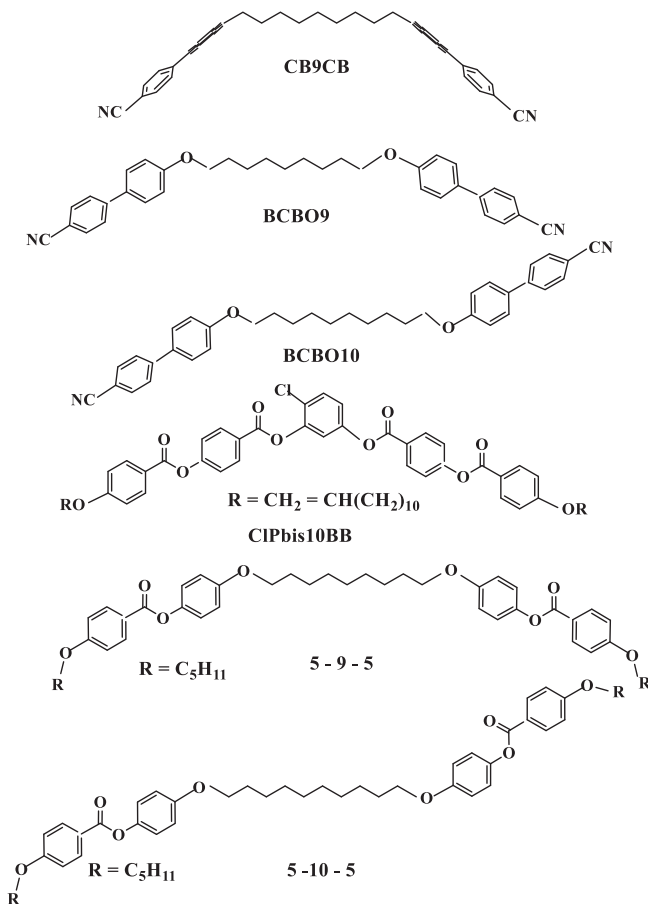


FIG. 13. Bent- and Z-shaped mesogens.

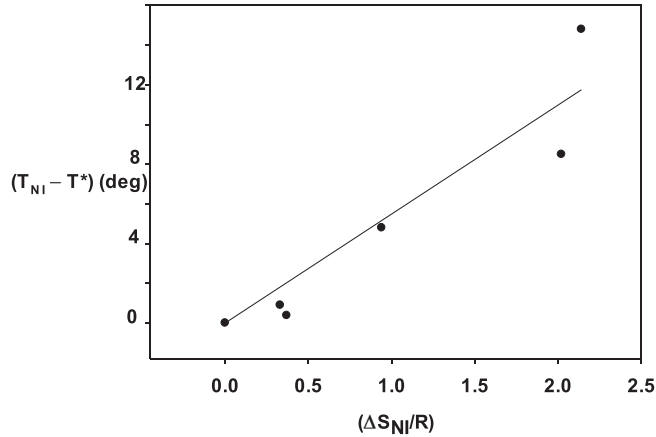


FIG. 14. The variation of $(T_{NI} - T^*)$ with $\Delta S_{NI}/R$ the change in entropy at T_{NI} for the mesogens in Table V. The straight line passing through the origin is a least-squares, linear fit to the data.

to both geometry and orientational order by

$$\begin{aligned}
 D_{i,j}(n) = & -K_{i,j}(n)\{S_{zz}(n)(3\cos^2\theta_{ijz} - 1) \\
 & + [S_{xx}(n) - S_{yy}(n)](\cos^2\theta_{ijx} - \cos^2\theta_{ijy}) \\
 & + 4S_{xy}(n)\cos\theta_{ijx}\cos\theta_{ijy} + 4S_{xz}(n)\cos\theta_{ijx}\cos\theta_{ijz} \\
 & + 4S_{yz}(n)\cos\theta_{ijy}\cos\theta_{ijz}\}, \quad (25)
 \end{aligned}$$

where

$$K_{i,j}(n) = \frac{\mu_0\gamma_i\gamma_j h}{32\pi^3 r_{ijn}^3}. \quad (26)$$

The angles $\theta_{ij\alpha}$ are between an axis α and the internuclear vector r_{ijn} fixed in a common reference frame x,y,z in each

TABLE VI. The values of D_{CH}^B and D_{HH}^B for the paranematic phase of CB9CB at 395.0 K with the atom labels as in Fig. 1.

i, j	$D_{CH_j}^B/\text{Hz}$	i, j	$D_{H_i H_j}^B/\text{Hz}$
3, 15 = 7, 18	5.8 ± 0.1	15, 16 = 17, 18	-21.4 ± 0.5
4, 16 = 6, 17	6.7 ± 0.1	28, 29	32.6 ± 0.5
8, 19 = 12, 22	9.8 ± 0.1	30, 31	11.43 ± 0.05
9, 20 = 11, 21	8.9 ± 0.1		
23, 28 = 23, 29	29.45 ± 0.05		
24, 30 = 24, 31	17.15 ± 0.05		
25, 32 = 25, 33	22.13 ± 0.05		
26, 34 = 26, 35	19.50 ± 0.05		
27, 36 = 27, 37	20.60 ± 0.05		

conformation. The field-induced dipolar couplings $D_{i,j}^B$ also obey Eqs. (24) and (25).

The spectra obtained at a temperature of 395.0 K, which is in the region where the paranematic and N_U phases coexist, are shown in Fig. 15 and were used to obtain a set of values of D_{CH}^B and D_{HH}^B at this fixed temperature. The values of $D_{C_i H_j}^B$ at 395.0 K are given in Table VI and shown in Fig. 16.

A. Structure and orientational order parameters for the cyanobiphenyl group

The values of $D_{C_i H_j}^B$ and $D_{H_i H_j}^B$ can be used to investigate the structure of CB9CB in exactly the same way as used for molecules in a uniaxial liquid crystal phase, as illustrated previously with data obtained in the pretransitional region for 5CB [11] and 5OCB and MBBA [12]. The values of $D_{C_i H_j}^B$ and $D_{H_i H_j}^B$ at 395.0 K in the molecular fragment shown in Fig. 17 are compared with values calculated from Eq. (25) modified

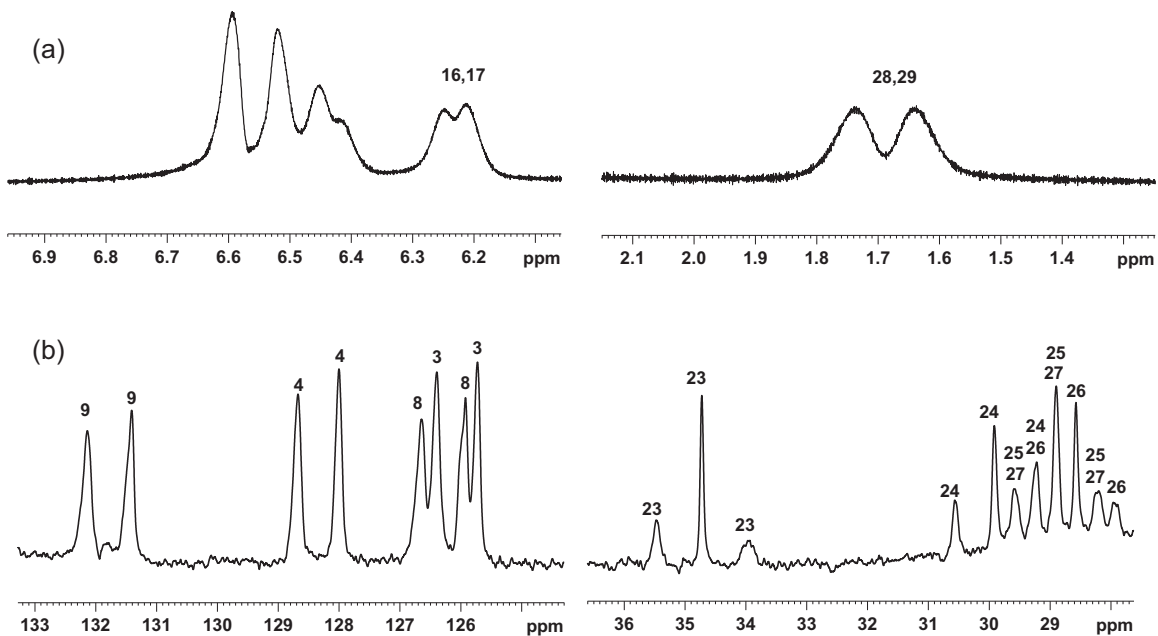


FIG. 15. (a) 1000-MHz ^1H and (b) 250-MHz ^{13}C spectra at a field of 23.5 T for selected regions of the spectrum measured for CB9CB at 395.0 K.

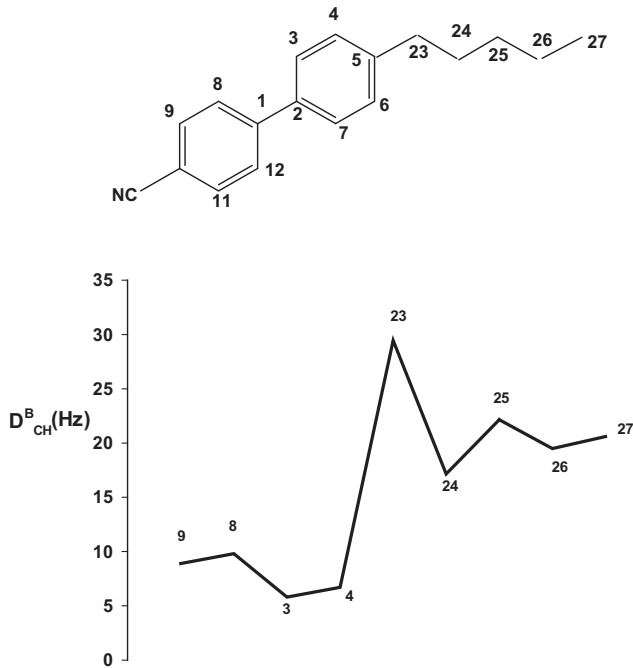


FIG. 16. The site dependence of $D_{\text{C,H}}^B$ for CB9CB in the paranematic phase at 395.0 K.

for a single conformation:

$$D_{i,j}^B = -K_{ij} [S_{zz}^B (3\cos^2\theta_{ijz} - 1) + (S_{xx}^B - S_{yy}^B) \times (\cos^2\theta_{ijx} - \cos^2\theta_{ijy}) + 4S_{yz}^B \cos\theta_{ijy} \cos\theta_{ijz}], \quad (27)$$

where the order parameters $S_{\alpha\beta}^B$ are for CB9CB molecules in the paranematic phase.

In any investigation using residual dipolar couplings there is always too little experimental data to investigate the structure, orientational order, and the potentials governing internal modes of motion, and so some simplifying assumptions are necessary. For the cyanobiphenyl-CH₂ fragment internal motion is approximated as involving the ring attached to the nitrile group rotating about the C₁-C₂ bond through a dihe-

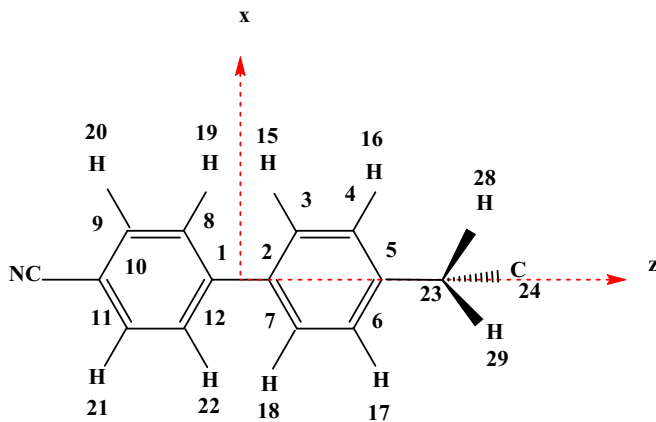


FIG. 17. The cyanobiphenyl-CH₂ fragment. The axes xyz are fixed in the alkylated ring with x and z in the ring plane.

TABLE VII. Values of the order parameters $S_{\alpha\beta}^B$ and the angles, $\theta_{a,b,c}$ /degrees, obtained for the biphenyl-CH₂ fragment by bringing calculated values of D_{ij}^B into best least-squares agreement with those observed.

$\theta_{15,3,2} = \theta_{18,7,2} = 116.9 \pm 1^a$
$\theta_{16,4,3} = \theta_{17,6,7} = 121.4 \pm 1$
$\theta_{19,8,9} = \theta_{22,12,11} = 119.2 \pm 1$
$\theta_{20,9,8} = \theta_{21,11,12} = 120.3 \pm 1$
$S_{zz}^B = 0.00289 \pm 0.00003^a$
$S_{xx}^B - S_{yy}^B = 0.000047 \pm 0.000002$
$S_{yz}^B = S_{zy}^B = -0.000643 \pm 0.000006$

^aErrors are estimated from errors in the measured values of D_{ij}^B .

dral angle $\delta_{8,1,2,3}$ between four minimum energy positions, while the alkyl chain rotates about the C₅-C₂₃ bond through a dihedral angle $\delta_{24,23,5,4}$ between two, equivalent minimum energy positions. Values of D_{ij}^B for i and j in different phenyl rings, or in the CH₂ and either ring, were not observed with the consequence that the two rings can be treated as being coplanar, with the CH₂ group fixed in either minimum energy form, that is, above or below the xz plane. The bond lengths and angles are assumed to be invariant to the internal modes of motion and at first are approximated as those calculated by the DFT quantum-chemical method for the same group in CB7CB [29].

With this set of assumptions there are seven measured values of $D_{\text{C,H}}^B$ for nuclei in the cyanobiphenyl-CH₂ fragment and allowing values of S_{zz}^B , $S_{xx}^B - S_{yy}^B$, and $S_{yz}^B = S_{zy}^B$, the three independent order parameters required in Eq. (27), to vary in order to match calculated with observed dipolar couplings. This resulted in poor agreement between calculated and observed values of $D_{\text{C,H}}^B$, which is probably because the magnitudes of $D_{\text{C,H}}^B$ are very sensitive to the values of the bond angles $\theta_{15,3,2} = \theta_{18,7,2}$; $\theta_{16,4,3} = \theta_{17,6,7}$; $\theta_{19,8,9} = \theta_{22,12,11}$; $\theta_{20,9,8} = \theta_{21,11,12}$, when these are close to 125.3°. Note that this sensitivity of the D_{ij}^B to the geometry of the biphenyl group is also important when using values of $D_{i,j}$, or deuterium quadrupolar splittings $\Delta\nu_i$, to determine order parameters for samples in liquid crystal phases. Allowing these four angles also to vary gave almost exact agreement and produced the optimized values of the order parameters and angles shown in Table VII. Note that the optimized values of the geometric parameters will contain systematic errors stemming from the adoption of bond lengths and angles calculated by DFT, and the neglect of averaging over vibrational motion.

Note that the set of $D_{\text{C,H}}^B$ and $D_{\text{H,H}}^B$ available for the biphenyl-CH₂ group cannot test models for the effect of rotation of the CH₂ protons about the C₅-C₂₃ bond. The two protons in the CH₂ group are fixed in these calculations below the xz plane of the attached ring with the vector $\mathbf{r}_{28,29}$ parallel to the ring x axis. Rotation of these protons to the equivalent positions above the xz -ring plane reverses the sign of S_{yz} , but the calculated values of $D_{\text{C,H}}^B$ and $D_{\text{H,H}}^B$ are unchanged, so their values are consistent with the H₂₈ and H₂₉ protons jumping between the two equivalent positions.

B. Rotation about bonds in the nonane chain spacer

The values of $D_{i,j}^B$ obtained at 395.0 K can be used to test models for bond-rotational motion in the nonane spacer, using

$$D_{i,j}^B = \sum_{n=1}^N P^B(n) D_{i,j}^B(n), \quad (28)$$

where $P^B(n)$ is the probability that the molecule is in conformation n in the pretransitional, paranematic region. The values of $D_{i,j}^B(n)$ are related to both conformation-dependent order parameters $S_{\alpha\beta}^B(n)$ and molecular geometry by

$$D_{i,j}^B(n) = -K_{ij} \{ S_{zz}^B(n) (3\cos^2\theta_{ijz} - 1) + [S_{xx}^B(n) - S_{yy}^B(n)] \times (\cos^2\theta_{ijx} - \cos^2\theta_{ijy}) + 4S_{yz}^B(n) \cos\theta_{ijy} \cos\theta_{ijz} \}. \quad (29)$$

To apply Eqs. (28) and (29) requires the adoption of models for calculating the probabilities $P^B(n)$ and the conformation dependent order parameters $S_{\alpha\beta}^B(n)$; here we use the additive potential (AP) model [30] which has been applied to NMR data obtained for similar molecules in the liquid crystal phase as well as the magnetic-field-induced paranematic phase. A mean potential $U_{\text{mol}}^B(\beta, \gamma, n)$ is introduced, namely

$$U_{\text{mol}}^B(\beta, \gamma, n) = U_{\text{aniso}}^B(\beta, \gamma, n) + U_{\text{iso}}(n). \quad (30)$$

The term $U_{\text{aniso}}^B(\beta, \gamma, n)$ is purely anisotropic and vanishes when the molecules are not in an orientationally ordered environment, while $U_{\text{iso}}(n)$ survives the loss of order. The conformation-dependent order parameters $S_{\alpha\beta}^B(n)$ depend only on $U_{\text{aniso}}^B(\beta, \gamma, n)$, thus

$$S_{zz}^B(n) = Q(n)^{-1} \int_0^\pi \sin\beta d\beta \int_0^{2\pi} d\gamma \left[\frac{3}{2} \cos^2\beta - \frac{1}{2} \right] \times \exp[-U_{\text{aniso}}^B(\beta, \gamma, n)/RT], \quad (31)$$

$$S_{xx}^B(n) - S_{yy}^B(n) = Q(n)^{-1} \int_0^\pi \sin\beta d\beta \int_0^{2\pi} d\gamma [\sin^2\beta \cos 2\gamma] \times \exp[-U_{\text{aniso}}^B(\beta, \gamma, n)/RT], \quad (32)$$

with the orientational partition function

$$Q(n) = \int_0^\pi \sin\beta d\beta \int_0^{2\pi} d\gamma \exp[-U_{\text{aniso}}^B(\beta, \gamma, n)/RT]. \quad (33)$$

The mean potential $U_{\text{aniso}}^B(\beta, \gamma, n)$ for a molecule in the n th rigid conformation in a uniaxial liquid crystal phase may, in general, be expressed as

$$U_{\text{aniso}}^B(\beta, \gamma, n) = - \sum_{L,m} \varepsilon_{0,m}^{(L)}(n) C_{L,m}(\beta, \gamma), \quad (34)$$

where $C_{L,m}(\beta, \gamma)$ is a modified spherical harmonic of rank L and components m . The summation extends from $L = 2$ to ∞ and $m = -L$ to $+L$ in steps of 1, but when used for calculating second-rank quantities, such as the order parameters, it is a good approximation to include only those terms having $L = 2$. The order parameters for molecules in the paranematic region

are ~ 100 times smaller than for the nematic phase, with the consequence that the equivalent expansion of Eq. (34) for $U_{\text{aniso}}^B(\beta, \gamma, n)$ is essentially exact when truncated at the terms with rank = 2. Thus,

$$U_{\text{aniso}}^B(\beta, \gamma, n) = - \sum_m \varepsilon_{0,m}^{(2)}(n) C_{2,m}(\beta, \gamma). \quad (35)$$

Even the simplest model for the conformations that can be populated for CB9CB has 81 conformations in each half of the symmetric dimer. In the AP model a further simplification of Eq. (34) is introduced in which the coefficients $\varepsilon_{0,m}^{(2)}(n)$ depend on the structure of each conformation, and this is achieved by relating the conformation-dependent coefficients $\varepsilon_{0,m}^{(2)}(n)$ to fragment specific ones, $\varepsilon_{m,p}^{(2)}(j)$, by

$$\varepsilon_{0,m}^{(2)}(n) = \sum_j \sum_p \varepsilon_{m,p}^{(2)}(j) D_{p,m}^{(2)}(\Omega_{jn}), \quad (36)$$

where the Wigner functions $D_{p,m}^{(2)}(\Omega_{jn})$ depend on the orientation, Ω_{jn} , of fragment j in the molecular reference frame in conformation n .

The probability of the n th conformation when the molecule is in the pretransitional region is obtained from

$$P^B(n) = (Q(n) \exp\{-[U_{\text{int}}(n)]/RT\})/Z, \quad (37)$$

with

$$Z = \sum_{n=1}^N \int_0^\pi \sin\beta d\beta \int_0^{2\pi} d\gamma \exp\{-[U_{\text{mol}}^B(\beta, \gamma, n)]/RT\}, \quad (38)$$

while $P_{\text{iso}}(n)$, the probability that a molecule is in conformation n when there is no orientational order, is given by

$$P_{\text{iso}}(n) = \exp[-(U_{\text{iso}}(n))/RT] / \sum_{n=1}^N \exp[-(U_{\text{iso}}(n))/RT], \quad (39)$$

which for molecules in liquid crystal phases may differ from $P^B(n)$, but when the molecules are in the paranematic phase, where their orientational order is very small, it is expected that $P^B(n)$ will be essentially equal in value to $P_{\text{iso}}(n)$.

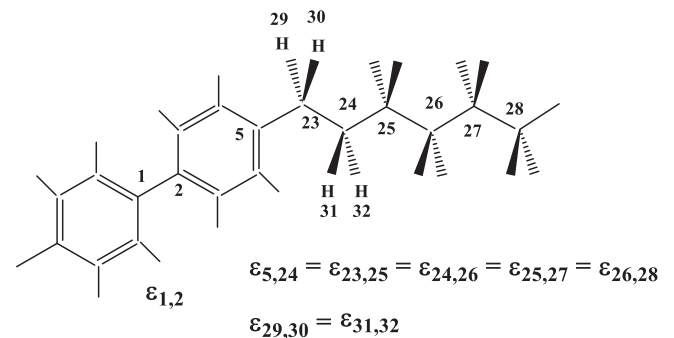
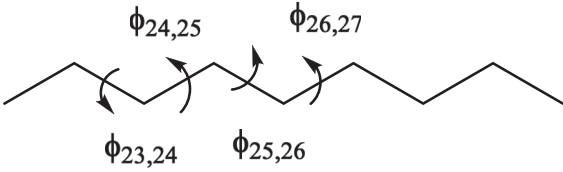


FIG. 18. Fragment interaction parameters $\varepsilon_{i,j}$ used for CB9CB when comparing the observed values of $D_{i,j}^B$ with those calculated by the AP method.

TABLE VIII. Energies, $E_{\min}/\text{kJ mol}^{-1}$, of the minimum energy forms generated for the symmetric nonane spacer in CB9CB by rotation about a bond $C_i - C_j$ through an angle $\phi_{i,j}/^\circ$, given by Emsley *et al.* [13].



$\phi_{23,24}$	E_{\min}	$\phi_{24,25}$	E_{\min}	$\phi_{25,26}$	E_{\min}	$\phi_{26,27}$	E_{\min}
180	0	180	0	180	0	180	0
± 115	2.6	± 112	4.0	± 115	3.8	± 115	3.8

C. Calculation of $P^B(n)$ for molecules of CB9CB from values of D_{ij}^B obtained at 395.0 K

The molecule CB9CB was divided into the fragments shown in Fig. 18, together with the fragment interaction parameters $\varepsilon_{i,j}$ used to construct the $\varepsilon_{m,p}^{(2)}(j)$ in Eq. (36).

The structure of the biphenyl- CH_2 fragment is that optimized above; the bond lengths and angles in the nonane spacer are assumed equal to those calculated by DFT for the same spacer in the symmetric dimer DTC5C9 by Emsley *et al.* [13]. The conformational distribution of an isolated molecule of CB9CB was approximated as being between the minimum energy conformations generated by rotations about the bonds, $C_i - C_j$ through angles $\phi_{i,j}$ shown in Table VIII.

The values for three independent fragment interaction parameters were varied to bring the calculated values of seven independent values of $D_{i,j}^B$ obtained at 395.0 K into best least-squares agreement with an rms error of 1.0 Hz. The optimized values of the $\varepsilon_{i,j}$ are given in Table IX.

The quality of the fit measured by the size and distribution of the differences $D_{i,j}^B(\text{calc.}) - D_{i,j}^B(\text{obs.})$, is good but not perfect. The values of these differences could be reduced by varying some bond lengths and angles in the nonane spacer, but this would not be a useful exercise given the sparsity of

TABLE IX. Optimized values of the fragment interaction parameters $\varepsilon_{i,j}/RT$ used to obtain the best least-squares agreement between calculated and observed values of $D_{i,j}^B$ for CB9CB at 395.0 K.

Optimized values of the fragment interaction coefficients:

$$\varepsilon_{1,2}/RT = 0.0134 \pm 0.0005$$

$$\varepsilon_{5,24}/RT = \varepsilon_{23,25}/RT = \varepsilon_{24,26}/RT = \varepsilon_{25,27}/RT = \varepsilon_{26,28}/RT = 0.00244 \pm 0.00001$$

$$\varepsilon_{29,30}/RT = \varepsilon_{31,32}/RT = 0.0023 \pm 0.0002$$

Calculated and observed $D_{i,j}^B$:

i, j	$D_{i,j}^B(\text{obs.})/\text{Hz}$	$D_{i,j}^B(\text{calc.})/\text{Hz}$	$[D_{i,j}^B(\text{calc.}) - D_{i,j}^B(\text{obs.})]/\text{Hz}$
15, 16 = 17, 18	-21.4 ± 0.5	-22.7	-1.3
28, 29	32.6 ± 0.5	30.8	-1.8
30, 31	11.43 ± 0.5	12.42	0.99
23, 28 = 23, 29	29.45 ± 0.05	29.05	-0.40
24, 30 = 24, 31	17.15 ± 0.05	18.46	1.31
25, 32 = 25, 33	22.13 ± 0.05	22.50	0.37
26, 34 = 26, 35	19.50 ± 0.05	19.24	-0.26
27, 36 = 27, 37	20.60 ± 0.05	19.43	-1.17

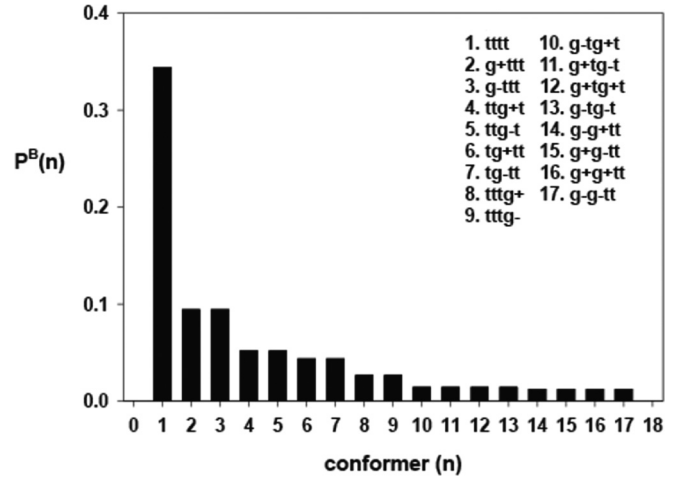


FIG. 19. The probabilities $P^B(n)$ of the 17 most populated conformers in the nonane spacer of CB9CB predicted to exist by the DFT calculations in the magnetic-field-induced paranematic phase at 395.0 K.

the experimental data compared with the number of structural unknowns. The very small values of the fragment interaction parameters mean that in the AP calculations the distributions $P^B(n)$ and $P_{\text{iso}}(n)$ obtained from Eqs. (37) and (39) are practically equal. It is possible, therefore, to conclude only that the set of $D_{i,j}^B$ available from the spectra recorded at 395.0 K is consistent with the distribution of conformers in the paranematic phase predicted for $P_{\text{iso}}(n)$ by the DFT calculations.

The discrete distribution of the 17 most populated conformers predicted by the DFT calculations is shown in Fig. 19.

VII. CONCLUSIONS

The bulk sample of CB9CB used here for our NMR experiments at 23.5 T has phase transitions at temperatures which are within experimental error ($\sim 1^\circ\text{C}$) of those measured in the Earth's magnetic field. This behavior is in marked contrast to the experiments by Salili *et al.* [6] on CB9CB which

monitored the effect of a magnetic field on the phase transitions by changes in its optical birefringence. These experiments were performed on samples contained between a pair of parallel glass plates separated by $5\ \mu\text{m}$ and surface treated to produce uniform planar alignment. In contrast the NMR spectra reported here used CB9CB contained in a cylindrical tube with a distance between its glass surfaces of $\sim 2\ \text{mm}$ and so can be considered to be free from surface forces.

The applied magnetic field produces a small, partial alignment of the molecules when the sample is above T_{NI} , which gives rise to field-induced dipolar couplings D_{CH}^B and D_{HH}^B . When the sample temperature is $\gg T_{\text{NI}}$ the magnitude of this partial alignment depends only on $\Delta\chi B^2$, and is equivalent to that obtained for molecules dissolved in isotropic solvents [31,32], but when the temperature is close to T_{NI} and the sample is in the paranematic phase, the values of the field-induced dipolar couplings are dominated by anisotropic, intermolecular forces and now D_{CH}^B and D_{HH}^B are predicted [21] and found to depend on temperature via $(T - T^*)^{-1}$. The highest temperature accessed in our NMR experiments on CB9CB was $145\ ^\circ\text{C}$ at which point the values of some of the D_{CH}^B and D_{HH}^B are small ($\sim 1\ \text{Hz}$), but measurable. On cooling from $145\ ^\circ\text{C}$ the values of D_{CH}^B and D_{HH}^B followed the expected dependence on temperature as the transition to the nematic phase N_{U} was approached. It was established that the same value of T^* is obtained for ten measured values of D_{ij}^B , giving an average value of $(T_{\text{NI}} - T^*) = 0.9 \pm 0.1\ ^\circ\text{C}$ which is between that of $0.38\ ^\circ\text{C}$ found for a bent-core ne-

matogen and a mean value of $1.7\ ^\circ\text{C}$ found for calamitic nematogens [22].

Values of D_{CH}^B and D_{HH}^B obtained at a fixed temperature of $395.0\ \text{K}$ were used to investigate the structure and orientational order of CB9CB when the sample is in the paranematic phase, including the distribution of conformations $P^B(n)$ adopted by the nonane spacer. This distribution is essentially identical to that predicted by quantum-mechanical calculations for an isolated molecule of CB9CB.

ACKNOWLEDGMENTS

We thank Dr. A. Jáklí for communicating to us recently that a calibration error in the work reported in Ref. [6] is responsible for the discrepancy between their results and ours. We are grateful to the IR-RMN project for enabling access to the 1000-MHz spectrometer in the Centre de Résonance Magnétique Nucléaire à Très Hauts Champs de Lyon. Very helpful discussions are acknowledged with Dr. I. Dozov of Laboratoire de Physique des Solides, UMR 8502 CNRS-Université Paris-Sud, Orsay, France, and Dr. C. Meyer of PSC, Université de Picardie Jules Verne, Amien, France. We also wish to thank Dr. B. A. Timimi of the School of Chemistry, Faculty of Engineering and Physical Sciences, University of Southampton, Southampton, UK, for valuable discussions of the thermodynamic theory by Prof. Rosenblatt. M.L. acknowledges Fondazione CR Firenze for funding support.

-
- [1] C. Rosenblatt, Magnetic field dependence of the nematic-isotropic transition temperature, *Phys. Rev. A* **24**, 2236 (1981).
- [2] D. H. Everett, *An Introduction to the Study of Chemical Thermodynamics*, 2nd ed. (Longman Group Limited, London and Harlow, 1971), p. xviii.
- [3] T. Ostapenko, D. B. Wiant, S. N. Sprunt, A. Jáklí, and J. T. Gleeson, Magnetic-Field Induced Isotropic to Nematic Liquid Crystal Phase Transition, *Phys. Rev. Lett.* **101**, 247801 (2008).
- [4] G. R. Luckhurst, C. Zannoni, P. L. Nordio, and U. Segre, A molecular field theory for uniaxial nematic liquid crystals formed by non-cylindrically symmetric molecules, *Mol. Phys.* **30**, 1345 (1975).
- [5] O. Francescangeli, F. Vita, F. Fauth, and E. T. Samulski, Extraordinary Magnetic Field Effect in Bent-Core Liquid Crystals, *Phys. Rev. Lett.* **107**, 207801 (2011).
- [6] S. M. Salili, M. G. Tamba, S. N. Sprunt, C. Welch, G. H. Mehl, A. Jáklí, and J. T. Gleeson, Anomalous Increase in Nematic-Isotropic Transition Temperature in Dimer Molecules Induced by a Magnetic Field, *Phys. Rev. Lett.* **116**, 217801 (2016).
- [7] T. B. T. To, T. J. Sluckin, and G. R. Luckhurst, Biaxiality-induced magnetic field effects in bent-core nematics: Molecular-field and Landau theory, *Phys. Rev. E* **88**, 062506 (2013).
- [8] N. Ghoshal, K. Mukhopadhyay, and S. K. Roy, Effect of an external magnetic field on the nematic-isotropic phase transition in mesogenic systems of uniaxial and biaxial molecules: A Monte Carlo study, *Phys. Rev. E* **89**, 042505 (2014).
- [9] P. A. Lebwohl and G. Lasher, Nematic-liquid-crystal order - A Monte-Carlo calculation, *Phys. Rev. A* **6**, 426 (1972).
- [10] D. A. Paterson, J. P. Abberley, W. T. A. Harrison, J. M. D. Storey, and C. T. Imrie, Cyanobiphenyl-based liquid crystal dimers and the twist-bend nematic phase, *Liq. Cryst.* **44**, 127 (2017).
- [11] D. Merlet, A. Lesage, and J. W. Emsley, Magnetic field induced dipolar couplings in the pretransitional region of a nematic liquid crystal, *J. Phys. Chem. A* **109**, 5070 (2005).
- [12] G. De Luca, J. W. Emsley, A. Lesage, and D. Merlet, The structures and conformations of mesogenic molecules in the pre-transitional region of the isotropic phase: 5OCB and MBBA and their mixtures, *Liq. Cryst.* **39**, 211 (2012).
- [13] J. W. Emsley, M. Lelli, H. Joy, M.-G. Tamba, and G. H. Mehl, Similarities and differences between molecular order in the nematic and twist-bend nematic phases of a symmetric liquid crystal dimer, *Phys. Chem. Chem. Phys.* **18**, 9419 (2016).
- [14] J. W. Emsley, M. Lelli, G. R. Luckhurst, and H. Zimmermann, ^{13}C NMR study of the director distribution adopted by the modulated nematic phases formed by liquid-crystal dimers with odd numbers of atoms in their spacers, *Phys. Rev. E* **96**, 062702 (2017).
- [15] J. Jeener and G. Alewaeters, Pulse pair technique in high resolution NMR, a reprint of the historical 1971 lecture notes on two-dimensional spectroscopy, *Prog. Nucl. Magn. Reson. Spectrosc.* **94-95**, 75 (2016); A. A. Shaw, C. Salaun, J.-F. Dauphin, and B. Ancian, Artefact-free PFG-enhanced double-quantum-filtered COSY experiments, *J. Magn. Reson. A* **120**, 110 (1996); B. Ancian, I. Bourgeois, J.-F. Dauphin, and

- A. A. Shaw, Artefact-free pure absorption PFG-enhanced DQF-COSY spectra including a gradient pulse in the evolution period, *ibid.* **125**, 348 (1997).
- [16] A. L. Davis, J. Keeler, E. D. Laue, and D. Moskau, Experiments for recording pure-absorption heteronuclear correlation spectra using pulsed field gradients, *J. Magn. Reson.* **98**, 207 (1992).
- [17] D.O. Cicero, G. Barbato, and R. Bazzo, Sensitivity enhancement of a two-dimensional experiment for the measurement of heteronuclear long-range coupling constants, by a new scheme of coherence selection by gradients, *J. Magn. Reson.* **148**, 209 (2001).
- [18] A. Bax, R. Freeman, and S. P. Kempell, Natural abundance carbon-13-carbon-13 coupling observed via double-quantum coherence, *J. Am. Chem. Soc.* **102**, 4849 (1980).
- [19] S. Berger and S. Braun, *200 and More NMR Experiments: A Practical Course* (Wiley-VCH Verlag GmbH & Co. KGaA, Weinheim, 2004); Bruker Variable Temperature Unit- User Manual. Version 001, Bruker SA, Wissembourg, France, 1998.
- [20] C. Ammann, P. Meier, and A. E. Merbach, A simple multinuclear NMR thermometer, *J. Magn. Reson.* **46**, 319 (1982).
- [21] N. J. Heaton and G. R. Luckhurst, Pretransitional behaviour in nematogens composed of flexible molecules. A molecular field theory, *Mol. Phys.* **66**, 65 (1989).
- [22] D. Wiant, S. Stojadinovic, K. Neupane, S. Sharma, K. Fodor-Csorba, A. Jáklí, J. T. Gleeson, and S. Sprunt, Critical behavior at the isotropic-to-nematic phase transition in a bent-core liquid crystal, *Phys. Rev. E* **73**, 030703(R) (2006).
- [23] G. S. Attard, P. A. Beckman, J. W. Emsley, G. R. Luckhurst, and D. L. Turner, Pretransitional behaviour in nematic liquid crystals. A nuclear magnetic resonance study, *Mol. Phys.* **45**, 1125 (1982).
- [24] D. A. Dunmur and M. R. Wilson, Light-scattering study of nematogenic molecules with a flexible core, *J. Chem. Soc. Faraday Trans. 2*, **84**, 1109 (1988).
- [25] K. Fodor-Csorba, A. Vajda, G. Galli, A. Jáklí, D. Demus, S. Holly, and E. Gács-Baitz, Ester-type banana-shaped monomers and investigations of their electro-optical properties, *Macromol. Chem. Phys.* **203**, 1556 (2002).
- [26] C. Rosenblatt, A. C. Griffin, U. Hari, and G. R. Luckhurst, Nematic-isotropic pretransitional behaviour in dimers with odd and even spacer lengths, *Liq. Cryst.* **9**, 831 (1991).
- [27] G. Sigaud, D. Y. Yoon, and A. C. Griffin, Order in the nematic phase of semi-flexible polymers, *Macromolecules* **16**, 875 (1983).
- [28] P. J. Collings and M. Hird, in *Introduction to Liquid Crystals, Chemistry and Physics* (Taylor and Francis Ltd., London, 1997), Chap. 12, p. 250.
- [29] J. W. Emsley, M. Lelli, A. Lesage, and G. R. Luckhurst, A comparison of the conformational distributions of the achiral symmetric liquid crystal dimer CB7CB in the achiral nematic and chiral twist-bend nematic phases, *J. Phys. Chem. B* **117**, 6547 (2013).
- [30] J. W. Emsley, G. R. Luckhurst, and C. P. Stockley, A theory of orientational ordering in uniaxial liquid crystals composed of molecules with alkyl chains, *Proc. R. Soc. London, A* **381**, 117 (1982).
- [31] J. A. B. Lohman and C. MacLean, Alignment effects on high resolution NMR spectra, induced by the magnetic field, *Chem. Phys.* **35**, 269 (1978).
- [32] L. M. Heist, C.-D. Poon, E. T. Samulski, D. Photinos, J. Jokisaari, J. Vaara, J. W. Emsley, S. Mamone, and M. Lelli, Benzene at 1 GHz. Magnetic field-induced fine structure, *J. Magn. Reson.* **258**, 17 (2015).